ACSNANO

www.acsnano.org

ARTICLE

Controlled Hysteresis of Conductance in Molecular Tunneling Junctions

Junwoo Park,[⊥] Mohamad S. Kodaimati,[⊥] Lee Belding, Samuel E. Root, George C. Schatz, and George M. Whitesides*

Cite This: *ACS Nano* 2022, 16, 4206–4216

Read Online

ACCESS | Metrics & More | Article Recommendations | Supporting Information

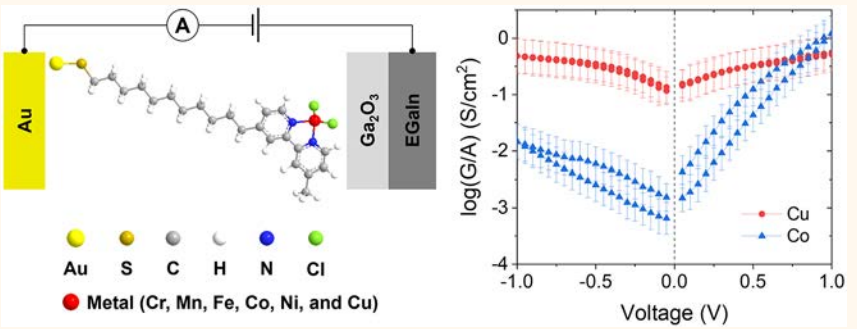

ABSTRACT: **The problem this paper addresses is the origin of the hysteretic behavior in two-terminal molecular junctions made from an EGaIn electrode and self-assembled monolayers of alkanethiolates terminated in chelates (transition metal dichlorides complexed with 2,2′-bipyridine; BIPY-MCl_2). The hysteresis of conductance displayed by these BIPY-MCl_2 junctions changes in magnitude depending on the identity of the metal ion (M) and the window of the applied voltage across the junction. The hysteretic behavior of conductance in these junctions appears only in an incoherent (Fowler−Nordheim) tunneling regime. When the complexed metal ion is Mn(II), Fe(II), Co(II), or Ni(II), both incoherent tunneling and hysteresis are observed for a voltage range between +1.0 V and −1.0 V. When the metal ion is Cr(II) or Cu(II), however, only resonant (one-step) tunneling is observed, and the junctions exhibit no hysteresis and do not enter the incoherent tunneling regime. Using this correlation, the conductance characteristics of BIPY-MCl_2 junctions can be controlled. This voltage-induced change of conductance demonstrates a simple, fast, and reversible way (i.e., by changing the applied voltage) to modulate conductance in molecular tunneling junctions.**

KEYWORDS: *charge transport, hysteresis in conductance, quantum tunneling, molecular tunneling junctions, self-assembled monolayers (SAMs), EGaIn junction, molecular electronics*

INTRODUCTION

One of the goals in the field of molecular electronics is the design of devices based on the structure and behavior of individual molecules. The development of such technology is aided by demonstrations of molecular junctions that exhibit the behavior of basic electronic components—e.g., molecular wires, rectifiers, memory devices, and transistors.[1−8] One key issue in the operation of the molecular electronic components is how to control the electrical *conductance* of a molecular junction. For example, *molecular wires* require high electrical conductivity along the molecule, across the interfaces between molecules, and between the molecules and the electrodes; *molecular rectifiers* require asymmetric conductance at opposite polarities; *molecular memory devices* use the change in conductance that arise from different physical states of the molecule to express information (0 or 1); and *molecular transistors* operate based on modulating the conductance through a junction by applying a gate voltage, which changes the energy level of molecular orbitals (MOs) involved in charge transport.

There have been many strategies applied in efforts to change the conductivity through a molecular junction (e.g., using various stimuli: changes in molecular geometry,[9−11] redox reactions,[12−15] pH,[16] magnetic field,[17] wavelength of light,[18,19]

Received: November 15, 2021
Accepted: February 11, 2022
Published: March 1, 2022

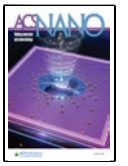

https://doi.org/10.1021/acsnano.1c10155
ACS Nano 2022, 16, 4206–4216

electric current,[20−22] and molecular vibration[23]).[24,25] Reliable rules, however, for relationships between the electronic structure in molecular junctions and hysteresis of conductance have been difficult to determine because comparisons of charge transport in molecules having different molecular structure are confounded by interrelated differences in contact geometry, packing density, orientation, and intermolecular interaction.[26]

Here, we investigate how the hysteresis in conductance in two-terminal molecular junctions made from self-assembled monolayers (SAMs) of alkanethiolates terminated in chelates (2,2′-bipyridine bound to first-row transition metal dichlorides; which we denote as BIPY-MCl_2 junctions on template-stripped Au with an EGaIn top electrode) correlates with the tunneling mechanism. BIPY-MCl_2 junctions are an excellent model system with which to investigate the hysteresis in conductance because the magnitude of hysteresis depends upon the identity of the metal ion (which is easy to change and produces approximately isostructural—by XPS—junctions). By changing the identity of the metal center in the BIPY-metal complex and the potential applied to the EGaIn electrode, we are able to change the energies of the frontier orbitals relative to the work functions of the electrodes to support our tunneling mechanism. This structural similarity allows us to perform a comparative study without the problems that arise when comparing other SAMs with different molecular structures.

RESULTS AND DISCUSSION

Hysteretic Behavior in BIPY-$CoCl_2$ and BIPY-$CuCl_2$ Junctions. Figure 1a shows the geometry of the molecular junctions: Au^{TS}-$S(CH_2)_{11}$BIPY-M(II)Cl_2//Ga_2O_3/EGaIn (we call the entire junction a "BIPY-MCl_2 junction"). The symbol "//" indicates a noncovalent interface, and "/" indicates the interface between EGaIn and Ga_2O_3. We used a template-stripped gold surface (Au^{TS}) as a bottom electrode[27] and a eutectic alloy formed between indium and gallium (75.5% Ga, 24.5% In, EGaIn) as a top electrode.[28−30] The molecular junctions are based on SAMs of alkanethiolates terminated by (we assume approximately isostructural) chelates—2,2′-bipyridine (BIPY) bound to transition metal chlorides (Cr(II), Mn(II), Fe(II), Co(II), Ni(II), or Cu(II)). The sulfur atom of the molecules forms a covalent bond with the gold surface (binding energy: ∼2 eV),[31] while the EGaIn electrode forms a noncovalent contact (we assume a van der Waals contact between Ga_2O_3 and bipyridyl complex) with the terminal BIPY-M(II)Cl_2 group of the SAM, without damaging the monolayer.[28] We apply voltages to the EGaIn electrode (the Au electrode is grounded) and measure charge transport (i.e., current) across a macroscopic area (∼1000 μm^2 of geometric area of contact of the SAMs with the EGaIn electrode).[29] On the basis of XPS results, incubating BIPY SAMs with either $CoCl_2$ or $CuCl_2$ forms BIPY-metal complexes with a 1:1 ratio of BIPY to metal (Table S1). We assume the complexation of a transition metal constrains the 2,2′-bipyridine group to a cis conformation and changes the electronic structure (e.g., the highest occupied molecular orbital (HOMO) and lowest unoccupied molecular orbital (LUMO)) of the aromatic portion of the SAM (the BIPY-metal complexes), depending on the transition metal.[32]

Figure 1b shows the dramatic difference in the characteristics of the tunneling current between Co and Cu (Figure 1b and Figure S1). The BIPY-$CoCl_2$ junctions display both hysteresis and rectification ($r^+ = |J(+V)|/|J(-V)| = 82$ at ±1.0 V), while the BIPY-$CuCl_2$ junctions do not exhibit either hysteresis or rectification at ±1.0 V ($r^+ = 1$). In addition to these differences

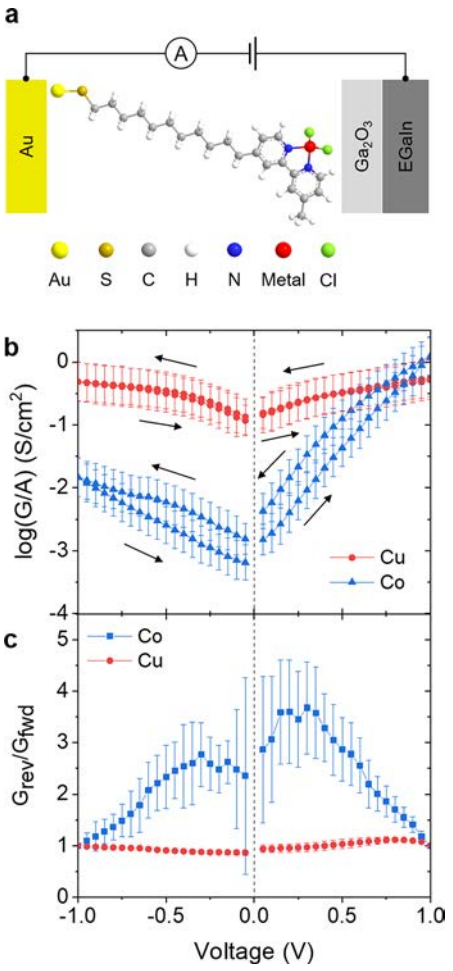

Figure 1. Geometry of junction, molecular design, and electrical characterization. (a) Schematic representation of the molecular tunneling junction composed of SAMs of 2,2′-bipyridine-terminated alkanethiolates: Au^{TS}-$S(CH_2)_{11}$BIPY-M(II)Cl_2//Ga_2O_3/EGaIn. (b) Averaged plots of conductance per unit contact area in log-scale versus applied voltage traces measured in BIPY-$CoCl_2$ and BIPY-$CuCl_2$ junctions. Black arrows indicate the direction (forward and reverse) in which the voltage was scanned. (c) The ratio of conductance for forward and reverse scan in Co and Cu junctions. The error bars represent the standard deviation: Co junctions (609 traces) and Cu junctions (525 traces).

in tunneling characteristics, the conductance through BIPY-$CoCl_2$ junctions at negative voltage is ∼100× lower than through BIPY-$CuCl_2$ junctions.

A dual functionality of rectification and hysteresis of conductance in the BIPY-$CoCl_2$ junction is useful in memristor-based arrays (e.g., resistive random-access memory).[33] An electronic component having both rectification and hysteresis of conductance is highly desirable because the deposition of a "selector"—which rectifies an undesired leakage current—into the arrays composed of a nonrectifying memristor (i) decreases the compactness of the array, (ii) increases the complexity of 3D interconnectivity, and (iii) increases the operating voltage.

We recently reported the mechanism for *rectification* in BIPY-MCl_2 junctions.[32] Our investigations indicated that rectification in BIPY-MCl_2 junctions is purely molecular in origin (e.g., is not due to asymmetry of the work functions of the electrodes) and is determined by the electronic structure of the SAM. The

https://doi.org/10.1021/acsnano.1c10155
ACS Nano 2022, 16, 4206−4216

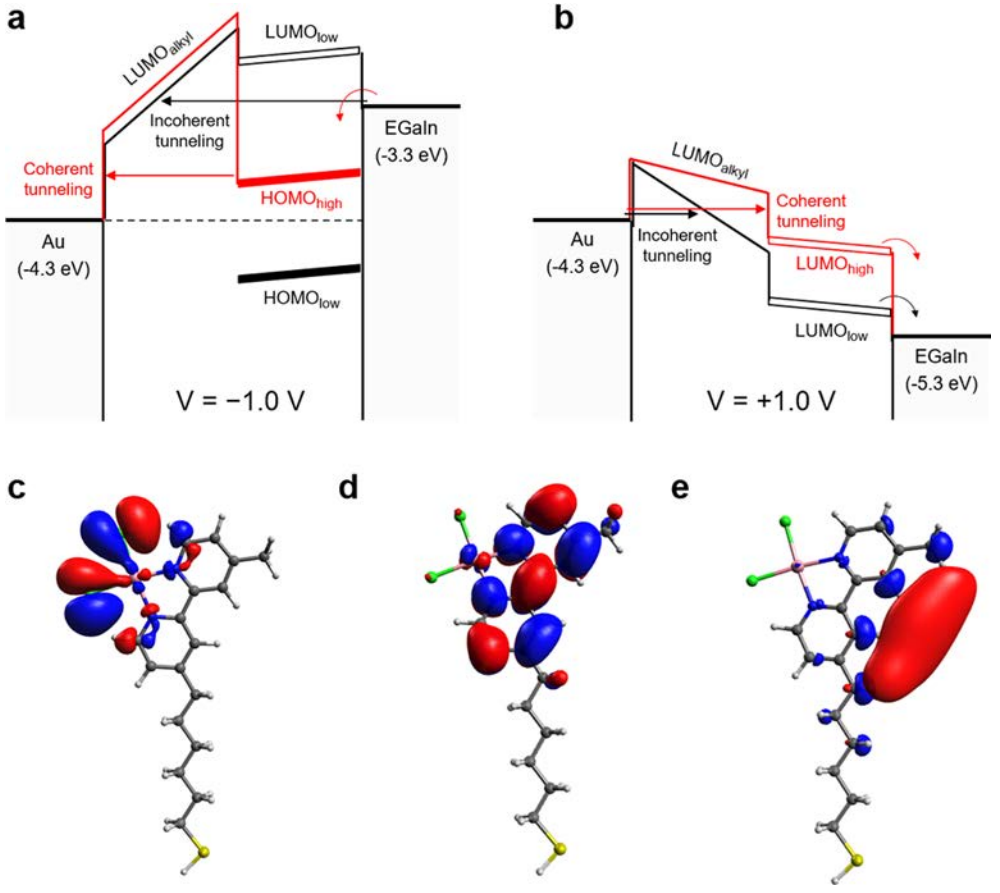

Figure 2. Schematic diagram of energy levels of molecular junctions: Au^{TS}-$S(CH_2)_{11}$BIPY-M(II)Cl_2//GaO_x/EGaIn at −1.0 V (a) and at +1.0 V (b).[32] The red lines indicate the potential barrier with decreased barrier height as the conduction mechanism of tunneling enters the incoherent tunneling regime. The solid rectangles and hollow rectangles, respectively, represent the HOMO and LUMO of conducting BIPY-MCl_2 complexes. BIPY-MCl_2 junctions complexed with Mn(II), Fe(II), Co(II), or Ni(II) have relatively low-lying (black) HOMOs and LUMOs, and BIPY-MCl_2 junctions complexed with Cr(II) and Cu(II) have relatively high-lying (red) HOMOs and LUMOs (details are in the main text). Geometry of orbitals for BIPY-$CoCl_2$ calculated by density functional theory (DFT) corresponding to the HOMO for the BIPY-$CoCl_2$ moiety (c), LUMO for the BIPY-$CoCl_2$ moiety (d), and the lowest-lying LUMO that is localized on the alkyl chain (e).

electronic structure in molecular junctions—specifically, the accessibility (whether the orbitals of the BIPY-metal complexes are involved in the tunneling process, based on their energy levels with respect to the energy levels of the electrodes) of the molecular orbital (MO) of the conducting moiety at a given voltage determines the occurrence of rectification and the mechanism of tunneling in BIPY-MCl_2 junctions (Figure 2). If the LUMO of the conducting moiety is accessible at +1.0 V and the HOMO is inaccessible at −1.0 V (e.g., BIPY-$CoCl_2$ junctions, Figure 2c−e), for example, the asymmetry in accessibility induces rectification, due to a difference in the width of the tunneling barrier at opposite polarities. On the other hand, molecular junctions (e.g., BIPY-$CuCl_2$ junctions) having a LUMO that is accessible at +1.0 V and HOMO that is accessible at −1.0 V do not rectify current because the tunneling barrier through the molecular junction is similar at ±1.0 V.

We have observed that the *conductance* (G ≡ I/V)—which is calculated as the ratio of the current that flows to the given voltage difference—changes in BIPY-$CoCl_2$ junctions in analysis of the forward scan (sweeping the voltage from −1.0 V to +1.0 V) in comparison to the reverse scan (sweeping the voltage from +1.0 V to −1.0 V). The conductance is larger for the reverse scan than for the forward scan. BIPY-$CuCl_2$ junctions, however, do not show a difference in conductance for the forward and reverse voltage sweeps (Figure 1b). Figure 1c shows the magnitude of hysteresis, expressed as the value of conductance for a given voltage during the reverse scan divided by the value of conductance for a given voltage during the forward scan—when there is no conductance hysteresis, G_{rev}/G_{fwd} = 1. These results clearly show a difference in the hysteresis between BIPY-$CoCl_2$ and BIPY-$CuCl_2$ junctions.

In BIPY-$CoCl_2$ junctions, the magnitude of conductance hysteresis (G_{rev}/G_{fwd}) converges to one (i.e., no difference in conduction) near the boundary of the voltage range we used (here, ± 1.0 V) and increases to a maximum value (G_{rev}/G_{fwd} = ~3.7 at +0.3 V) as the applied voltage decreases. We interpret this result to mean that the BIPY-$CoCl_2$ junctions allow 3.7 times more current density to flow across the molecule during the reverse scan than during the forward scan, at the same voltage of +0.3 V. In BIPY-$CuCl_2$ junctions, however, the magnitude of conductance during the forward scan and the reverse scan is nearly the same within the whole range of applied voltage and thus does not show hysteresis.

Various possible mechanisms for the change in conductance of the thiol junctions-terminated conjugated molecules have been proposed: reduction/oxidation of a particular functional group,[34] rotation of a functional group,[35] rotation of a conjugated backbone,[36] changes in intermolecular interac-

https://doi.org/10.1021/acsnano.1c10155
ACS Nano 2022, 16, 4206−4216

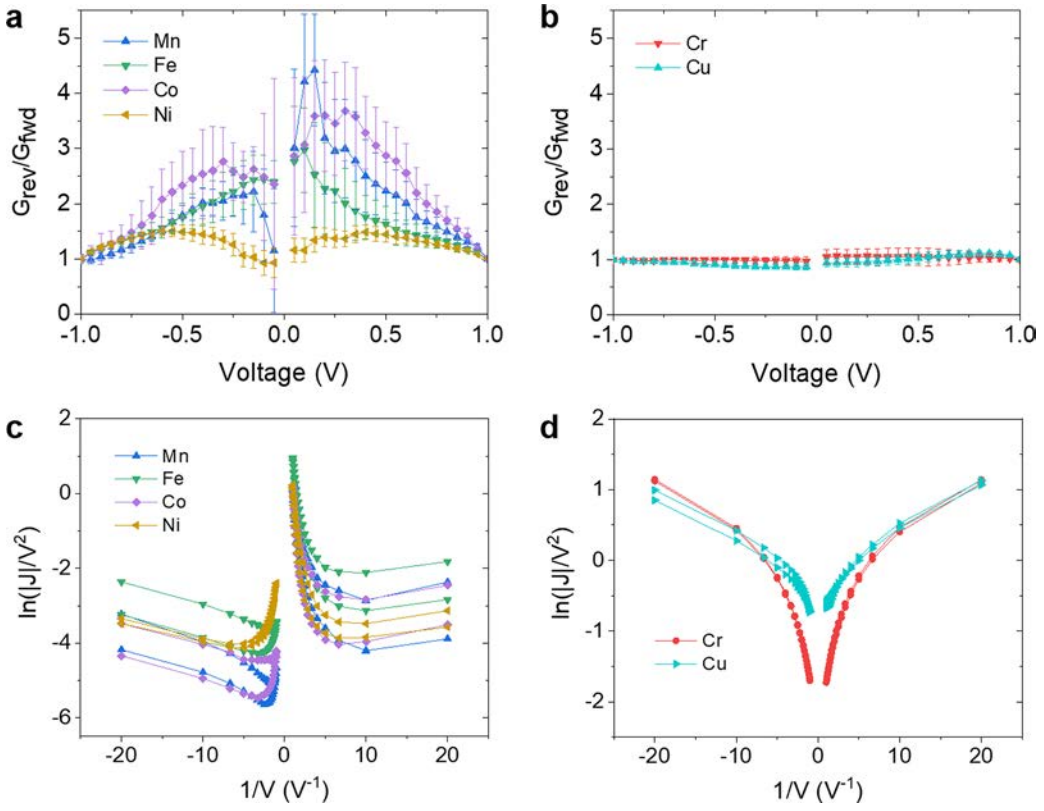

Figure 3. The occurrence of hysteresis and the mechanism of tunneling. The ratio of current densities for the forward and reverse scans in BIPY-MCl_2 junctions. (a) M = Mn, Fe, Co, and Ni. (b) M = Cr and Cu. Fowler−Nordheim (FN) plots for BIPY-MCl_2 junctions. (c) M = Mn, Fe, Co, and Ni. (d) M = Cr and Cu. BIPY-MCl_2 junctions complexed with Mn, Fe, Co, or Ni show the transition from coherent tunneling to incoherent tunneling. BIPY-$CrCl_2$ and BIPY-$CuCl_2$ junctions have no change in the mechanism of conductance within the range of applied voltages (−1.0 V to +1.0 V).

tions,[37] fluctuations in bond length,[38] changes in hybridization of metal-molecule bonds,[39] and counterion migration.[22] BIPY-$CuCl_2$ junctions, which undergo reduction and oxidation with applied voltages between −1.0 V to +1.0 V, do not show hysteresis.[32] Thus, we presume oxidation or reduction of the BIPY-$CuCl_2$ complex cannot be the origin of the change in conductance in BIPY-$CuCl_2$ or other junctions. Rotation about the central C−C bond (between the two pyridine groups) can also be excluded as a mechanism of hysteresis because both BIPY-$CoCl_2$ and BIPY-$CuCl_2$ have fixed conformations of the 2,2′-bipyridine group and have the same core structure (based on XPS and solution-phase experiments).[32,40] Further, we tested whether the halide anions, or the nature of the M−X bond, influence hysteresis in these systems by preparing BIPY-metal junctions using MCl_2, MI_2, and MBr_2 (Figure S2). We observed no change in the behavior of the junction upon change of halide counterion.

Correlation between Hysteresis in Conductance and the Mechanism of Tunneling. We expanded our analysis of the hysteresis in BIPY-MCl_2 junctions to include other first-row transition metals (Ni(II), Fe(II), Mn(II), Cr(II)) and observed a correlation between the hysteresis in conductance and the mechanism of tunneling (Figure 3). BIPY-MCl_2 junctions complexed with Mn, Fe, or Ni (like BIPY-$CoCl_2$ junctions) clearly show hysteresis, while those complexed with Cr (like BIPY-$CuCl_2$ junctions) do not. The mechanism of tunneling in BIPY-$CoCl_2$ junctions—which display hysteresis—is incoherent tunneling (specifically, Fowler−Nordheim tunneling, FN tunneling),[41] while the mechanism of tunneling in BIPY-$CuCl_2$ junctions—which do not display hysteresis—is resonant tunneling (Figure 3c,d). We believe that incoherent tunnelling is the operative mechanism of tunnelling for the BIPY-$CoCl_2$ junctions based on the following experimental observations: (i) the FN plots (Figure 3c) show a minimum—indicating a transition from one transport mechanism to another[42]—and a linear relationship $1/V$ and $\ln(|J|/V^2)$ at high voltages, (ii) the relative energies of the frontier orbitals determined by CV and UPS,[41] and (iii) the temperature dependence of tunnelling through the junctions.[41] We do not believe the linear relationship between $1/V$ and $\ln(|J|/V^2)$ is an artifact due to the construction of our junctions as we do not observe this relationship with BIPY-$CuCl_2$, BIPY-$CrCl_2$, or alkylthiol-functionalized SAMS (Figure S3). While we are unable to measure the HOMO−LUMO gap of the BIPY-MCl_2, we have measured the HOMO through UPS[41] and confirmed that the HOMO of BIPY-$CuCl_2$ is accessible at an applied potential of −1.0 V. From our temperature-dependent tunnelling experiments[41] at +1.0 V, we observed a thermally activated hopping step; the temperature dependence indicates that the LUMO is accessible as well. This correlation held for all BIPY-MCl_2 junctions that we investigated. BIPY-MCl_2 junctions (M = Mn(II), Fe(II), Co(II), or Ni(II)) that show the characteristics of conductance hysteresis (and rectification) show incoherent tunneling as the mechanism of tunneling at ±1.0 V, while for the junctions that exhibit no hysteresis and no rectification (M = Cr(II) or Cu(II)), the mechanism of tunneling is direct tunneling.

https://doi.org/10.1021/acsnano.1c10155
ACS Nano 2022, 16, 4206−4216

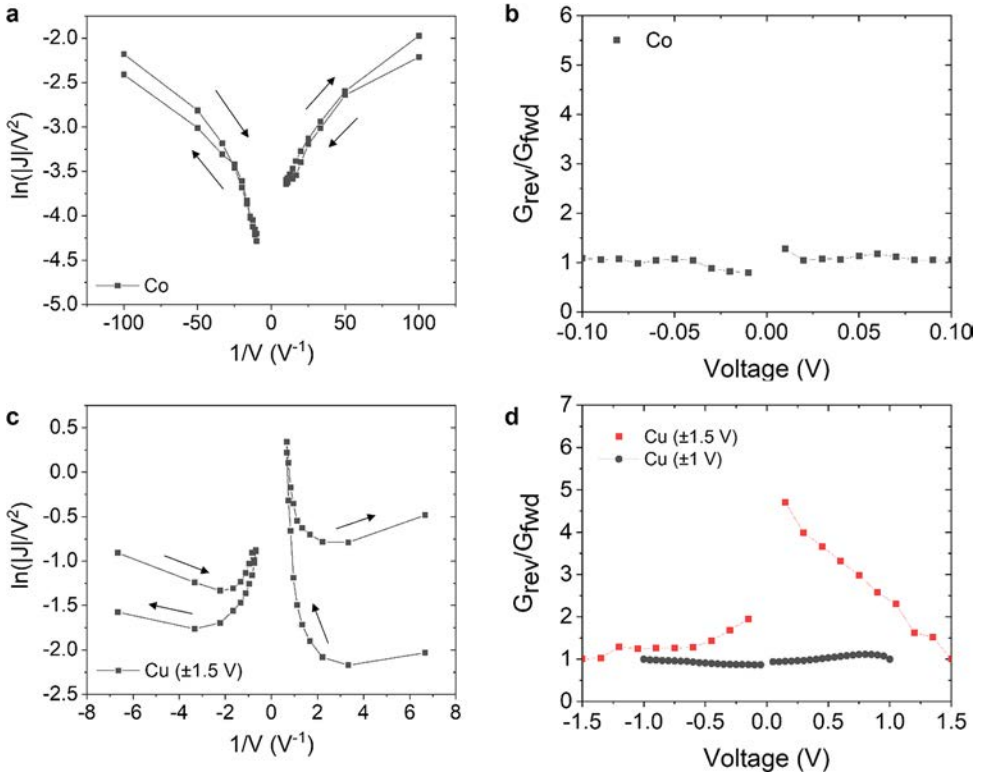

Figure 4. Controlled hysteresis of conductance in BIPY-MCl_2 junctions. Fowler−Nordheim plots and the magnitude of hysteresis (a and b) in BIPY-$CoCl_2$ junctions with a voltage window of ±0.1 V and (c and d) in BIPY-$CuCl_2$ junctions with a voltage window of ±1.5 V.

On the basis of these experimental results, we hypothesized that *the hysteretic behavior in BIPY-MCl_2 junctions appears only in the incoherent tunneling regime*. The difference between incoherent tunneling and coherent tunneling in BIPY-MCl_2 junctions is whether the electrons occupy the LUMO that is localized primarily on the alkyl chain, or not. If we consider charge transport in BIPY-$CoCl_2$ junctions at −1.0 V, for example, electrons in the incoherent tunneling regime tunnel to the LUMOs of the alkyl chains, while in BIPY-$CuCl_2$ junctions, electrons in the coherent tunneling regime at −1.0 V tunnel to the Fermi level of the Au electrode (Figure 2). Similarly, if we consider charge transport in BIPY-$CoCl_2$ junctions at +1.0 V, electrons incoherently tunnel through the junction in a two-step process: (i) tunneling through the LUMOs of the alkyl chains and (ii) hopping to the LUMO of the BIPY-$CoCl_2$ moiety. In BIPY-$CuCl_2$ junctions at −1.0 V, electrons coherently tunnel to the LUMO of the BIPY-$CuCl_2$ and then hop to the Fermi level of the Au electrode (Figure 2). As such, at +1.0 V, electrons will presumably spend more time occupying the LUMO of BIPY-$CoCl_2$ than BIPY-$CuCl_2$. While we do not believe that the LUMO orbitals of the alkyl chain are involved in a one-step tunneling process through the junction, we believe that the electron might tunnel through these orbitals using a two-step process involving a virtual-state originating from the LUMO orbital of the alkyl chain.[43]

EXPERIMENTAL EVIDENCE FOR OUR HYPOTHESIS

Controlled Hysteresis in Conductance in BIPY-MCl_2 Junctions. If our hypothesis is correct, we should be able to modulate the hysteresis in BIPY-MCl_2 junctions by decreasing the applied voltage window, in BIPY-$CoCl_2$ junctions, to the regime in which only coherent tunneling is observed. We thus reduced the range of applied voltages from ±1.0 V to ±0.1 V so that the mechanism of tunneling in BIPY-$CoCl_2$ junctions stays in the coherent tunneling regime (Figure 4a). Under these conditions, electrons do not occupy the LUMO of the alkyl chain and tunnel the whole width of the tunneling barrier between the Au and EGaIn electrodes. As we restrict the transition of the mechanism of tunnelling (by decreasing the applied voltage window to ±0.1 V), the hysteretic behavior in BIPY-$CoCl_2$ junctions—which are present in the voltage range from −1.0 V to +1.0 V—disappears (Figure 4b). Similarly, the mechanism of tunneling in BIPY-$CuCl_2$ junctions is coherent tunneling at ±1.0 V, and the junctions do not show a difference in conductance between the forward and reverse scan due to hysteresis. Upon increasing the range of applied voltage in BIPY-$CuCl_2$ junctions (from ±1.0 V to ±1.5 V), where the mechanism of tunneling changes from coherent tunneling to incoherent tunneling (Figure 4c), the junction started to exhibit hysteretic behavior (Figure 4d). Similarly, we re-examined the behavior of all tested BIPY-MCl_2 junctions, and we observed hysteresis only in the incoherent tunneling regime. This observation suggests a coupled relationship between the mechanism of tunnelling and the electronic structure that causes conductance hysteresis (Figure S4).

Positive Correlation between Hysteresis in Conductance and Rectification Ratio. Rectification in BIPY-MCl_2 junctions seems to originate from an asymmetry in accessibility of the MOs at two opposite polarities; this accessibility is determined by the energy levels of the MOs (HOMO and LUMO) of the conducting moiety at ±1.0 V.[32] In the BIPY-MCl_2 junctions complexed with Mn(II), Fe(II), Co(II), or Ni(II), the HOMO is lower in energy (*low-lying* HOMO) than the Fermi level of the Au surface (i.e., the HOMO is inaccessible) at −1.0 V, and the LUMO is lower in energy (*low-lying* LUMO) than the Fermi level of Au surface (i.e., the

https://doi.org/10.1021/acsnano.1c10155
ACS Nano 2022, 16, 4206−4216

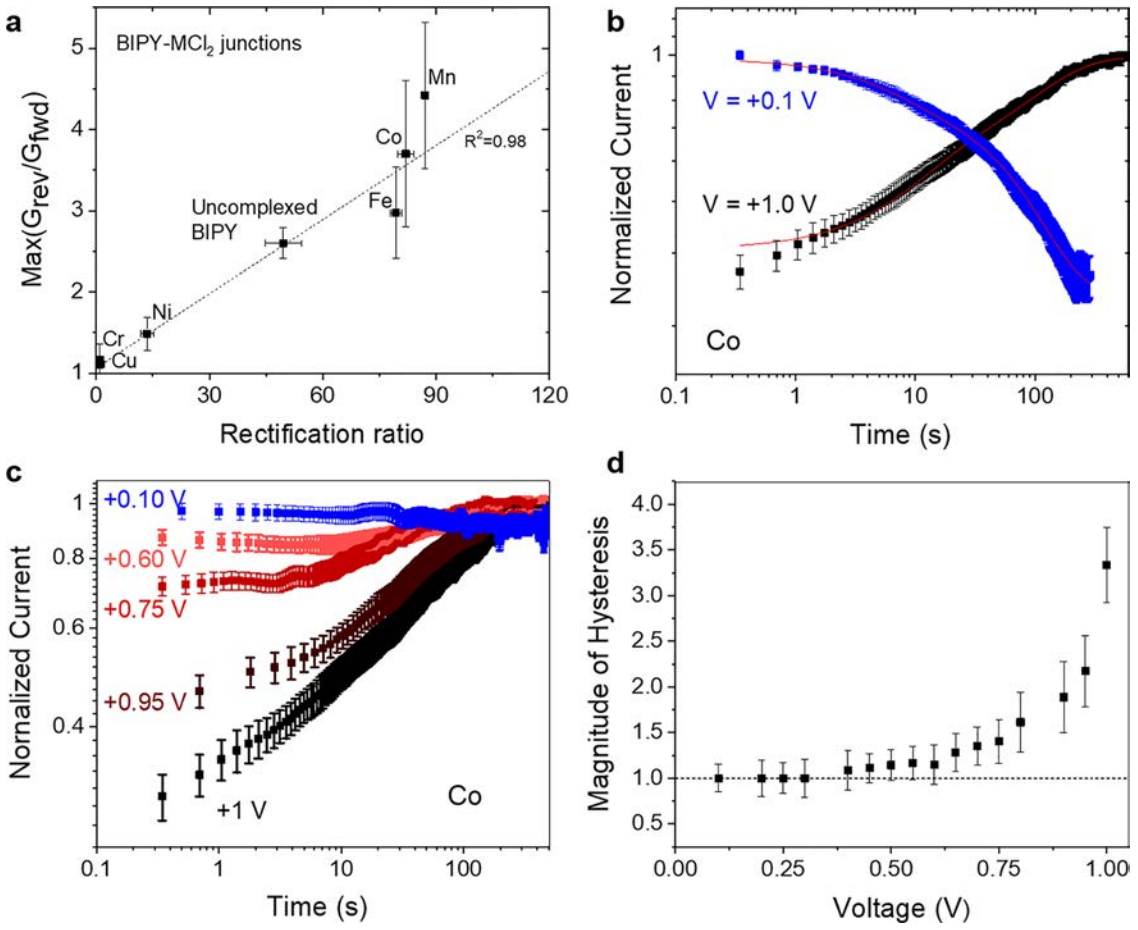

Figure 5. (a) A positive correlation between hysteresis of conductance and the rectification ratio. Each data point indicates the maximum values of hysteresis within the voltage range (−1.0 V to +1.0 V) and rectification ratios at ±1.0 V in BIPY-MCl_2 junctions where the labels denote the metal complexed to BIPY. Dashed lines are linear fit to the data. The oxidation state of these junctions was determined by XPS. (b) Amperometric data of BIPY-$CoCl_2$ junctions upon switching from 0 to 1 V (black squares) and switching from 1 to 0.1 V (blue squares). Red lines are fits to two first-order reactions as described in the main text. (c) Amperometric data of BIPY-$CoCl_2$ junctions at applied voltages of 1, 0.95, 0.75, 0.6, and 0.1 V. (d) Plot of magnitude of hysteresis as a function of applied voltage. Dashed line corresponds to no hysteresis (value of 1). Error bars in (b, c, and d) correspond standard error for measurements averaged over 7 different samples and 15 measurements per sample.

LUMO is accessible) at +1.0 V. Because of the difference in accessibilities of the orbitals at +1.0 V and −1.0 V, these junctions rectify current due to asymmetries in the tunneling widths at ±1.0 V (Figure 2).[32] BIPY-MCl_2 junctions complexed with Cr(II) and Cu(II) have relatively high-lying HOMOs and LUMOs, and almost identical widths of the tunneling barriers at ±1.0 V (Figure 2). These molecular junctions do not rectify current—rectification ratios ($(J(+V)/J(-V))$ for both junctions are ∼1.0—because both the HOMO is accessible at −1.0 V and the LUMO is accessible at +1.0 V. Therefore, a low-lying HOMO and a low-lying LUMO are the origin of rectification in BIPY-MCl_2 junctions.

The mechanism of tunneling is incoherent tunneling only when the energy of the HOMO is lower than the Fermi level of the Au electrode (low-lying HOMO) at −1.0 V and only when the barrier height at alkyl/BIPY-metal interface is lower than the Fermi level of the Au electrode at +1.0 V due to the low-lying LUMO. Thus, in BIPY-MCl_2 junctions, a low-lying HOMO at −1.0 V and a low-lying LUMO at +1.0 V are also the origin that causes the molecular junctions to enter the incoherent tunneling regime (Figure 2).

If the hysteretic behavior in BIPY-MCl_2 junctions appears only in the incoherent tunneling regime, according to our interpretation, the hysteresis should have a positive correlation with rectification because the rectification and hysteresis in conductance share the same origin in BIPY-MCl_2 junctions. Plots of the maximum value of conductance hysteresis (over a voltage range of −1.0 V to +1.0 V) versus the rectification ratio in BIPY-MCl_2 junctions show a *positive* correlation (R^2 = 0.98) between them (Figure 5a). This result implies experimental evidence for a strong relationship between the change in conductance and incoherent tunneling. The error bars represent the standard deviation: Cr (483 traces on 23 junctions, one trace 0 V → + 1.0 V → 0 V → −1.0 V → 0 V), Mn (483 traces on 23 junctions), Fe (483 traces on 23 junctions), Co (609 traces on 29 junctions), Ni (483 traces on 23 junctions), and Cu (525 traces on 25 junctions).

The hysteresis in $J-V$ traces of molecular rectifiers based on molecular tunneling junctions has been observed by previous measurements.[44−47] The hysteresis window of molecular rectifiers, however, has not received attention. We suggest that the experimental results—that is, a positive correlation between hysteresis in conductance and rectification—that we have observed in this study may be the cause of the hysteresis in conductance in other molecular rectifiers.

https://doi.org/10.1021/acsnano.1c10155
ACS Nano 2022, 16, 4206−4216

Characteristics of Incoherent Tunneling-Induced Conductance Hysteresis. We tested whether the dependence of the hysteresis on the applied voltage is path-dependent or path-independent (i.e., if the hysteresis is determined by the order in which the voltages are applied or solely the final voltage that is applied). We observed that scanning the voltage in a clockwise direction (i.e., 0 V → +1.0 V → 0 V → −1.0 V → 0 V) is similar to when we performed the measurement in a counterclockwise direction (i.e., 0 V → −1.0 V → 0 V → +1.0 V → 0 V) (Figure S5). That is, the junctions exhibit a lower current density for a forward scan than a reverse scan. This result leads us to believe that hysteresis can be attributed to the interaction of the tunneling electrons with the LUMO of the alkyl chain in BIPY-MCl_2 junctions during tunneling. We do not believe the electrons are occupying the LUMO of the alkyl chain or performing a redox reaction. There are three possible mechanisms for hysteresis that originate from differences between coherent and incoherent tunneling in terms of the way transport of electrons affects the charge transport in the junctions.

(I) First, electrons tunneling under incoherent tunneling conditions have greater incident kinetic energies than those undergoing coherent tunneling when they reach the opposite electrode because potential energy becomes kinetic energy (Figure S6). Energetic electrons can generate traps (e.g., an immobilized charge) at the surface of electrodes, and the trapping/detrapping process may cause the observed hysteretic behavior.[48−52] We performed experiments (Figure S7) in which we reduced the range of applied voltage from ±2.0 V to ±0.4 V (20 traces for each range) while keeping the number of voltage steps constant. We then measured the change of conductance in the range of ±1.6 V (orange dots). For the experiment with the voltage scanned over the window of ±2.0 V, the molecular junctions exhibit hysteresis (e.g., at +0.2 V, the magnitude of G_{rev}/G_{fwd} is 8.1). When a voltage window of ±0.4 V is used, no hysteresis is observed at the same voltage (+0.2 V). These results indicate that the hysteretic behavior is dependent upon the mechanism of conductance (i.e., whether the junctions undergo incoherent tunneling or not) and eliminates hypotheses associated with charge trapping/detrapping induced by energetic electrons.[48−52] The absence of charging effects in $J-V$ plots further supports this conclusion. Furthermore, as a voltage range ±1.6 V is applied to the same junction, there is hysteresis, indicating that the modulation of conductance and hysteresis in BIPY-MCl_2 junctions is *reversible*.

(II) The second possibility is that the electric field within the junction modifies the adhesion/contact area of the electrode, the conformational structure, and/or electronic structure of the BIPY-MCl_2 junctions. To test this hypothesis, we performed DFT calculations on BIPY-$CoCl_2$ and BIPY-$CuCl_2$ at zero electric field and electric fields up to 3 V/nm (Figure S7). When we compared the DFT results of BIPY-$CoCl_2$ and BIPY-$CuCl_2$ with no applied electric field and an electric field of 3 V/nm, we did not observe a measurable difference in their geometries or electron densities of the frontier orbitals. As such, we do not believe the hysteresis is due to the electric fields within the junction. We rule out changes in the adhesion/contact area of the electrode as the hysteresis is fully reversible (Figure S6) and occurs when the EGaIn electrode is encapsulated by an adhesive (Figure S8). We also do not suspect that hysteresis is due to ion migration as we observed that the reversal of the hysteresis in the presence of no applied potential or a low applied potential (0.1 V, Figure 5b) occurred at the same time scale as the building of hysteresis (∼100 s). For ion migration, we would expect the building of hysteresis to occur much faster than the reversal of the hysteresis.

(III) The third possibility is that, under incoherent tunneling conditions, electrons interacting with the LUMO of the alkyl chain affect the physical and/or electronic structure of the molecular tunneling junctions as the time the electrons reside in the LUMO is nonzero.[48] These interactions can either be (i) direct electronic or vibronic interactions of the tunneling electrons at the single-molecule level or (ii) indirect interactions due to thermal relaxation of electrons tunneling down the LUMO of the alkyl chain changing the conformational order of the SAMs[26] (akin to Joule heating). These two mechanisms can be distinguished by the time scales associated with generating hysteresis. Changes at the single-molecule level should occur on a time scale commensurate with molecular vibrations (∼picoseconds),[53] whereas the changes in the conformational order of the SAMs should occur on longer time scales.[54,55]

To measure the time scales of generating hysteresis, we performed amperometric measurements on BIPY-$CoCl_2$ junctions where we measured the current as a function of time for a given applied voltage. We performed amperometric measurements under an inert (N_2) atmosphere to prevent changes in the oxidation state of the EGaIn electrode over the course of a single experiment. When we switched from 0 to 1 V, we observed an increase in the current by a factor of ∼3.5 over the course of ∼400 s. If we then switched from 1 to 0.1 V, we observed a decrease in the current by a factor of ∼3.5 over the course of ∼400 s (Figure 5b). The kinetics of these processes does not follow simple power laws; the simplest kinetic model that we could use to fit these processes required two exponential (first-order) processes to describe the amperometric data (red curves in Figure 5b). Notably, the magnitude and building time for the hysteretic behavior increased with the applied voltage (Figure 5c), which is consistent with changes in the conformational order of the SAMs. From the amperometric data, we inferred that this process involves >2 conformational states; we did not attempt to derive additional information from these fits. The voltage required to generate hysteretic behavior (i.e., the threshold voltage) was ∼0.45 V (Figure 5d)—consistent with the voltage at which we began to observe the transition to the incoherent tunneling regime for the BIPY-$CoCl_2$ junctions (Figure 3a). When we performed voltage sweeps of the BIPY-$CoCl_2$ junctions, we observed the same trends as in the amperometric data—namely, the magnitude of hysteresis increased slowly over the course of ∼100s of seconds and increased with a higher applied voltage. (Figures S7 and S10). Furthermore, the hysteretic behavior of the BIPY-$CoCl_2$ junctions—which is present at room temperature—disappeared at 200 K. This result showed that conductance switching in the BIPY-$CoCl_2$ junctions is dependent upon temperature (Figure S9). From these experiments, we hypothesized that in the incoherent tunneling regime, tunneling electrons thermally relax—dissipating the excess energy into the SAMs and heating

https://doi.org/10.1021/acsnano.1c10155
ACS Nano 2022, 16, 4206−4216

the SAMs. At higher "temperatures", the molecular conformation of the SAMs changes—generating the hysteretic behavior. This hypothesis is consistent with previous reports of electronic heating in molecular junctions generating high temperatures in molecular junctions (>550 K).[56−60] The thermal conductance of molecular junctions is low (~10 pW K^{-1}) and is limited by the coupling of the phonon modes of the metals to vibrations of the molecule.[61−64] To confirm if the hysteresis involves conformational changes in the SAMs, we performed confocal Raman measurements on the BIPY-$CoCl_2$ junctions at 0 and 1 V (Figure S11). We observed changes in the Raman peaks (width, intensity, and energy) associated with the ring modes of 2,2-bipyridine.[65,66] When we applied a potential of 1 V, we observed broadening of many peaks (as compared to observations at 0 V), which indicates some conformational disorder. Ideally, one could measure the temperature of the SAMs by comparing the intensity of the anti-Stokes and Stokes peaks (Raman thermometry).[56,67,68] Recent work done by our group[26] and Thuo and co-workers[69] has highlighted the importance of conformational disorder on experimentally observed tunneling rates.[26,69] We suspect one possible mechanism for the hysteretic behavior in the BIPY-$CoCl_2$ junctions is that the increased conformation disorder decreases the thickness of the SAMs—increasing the tunneling current. An increase in the effective temperature of the junction would also increase the rate of incoherent tunneling and observed current. While tunneling through the junctions should still be fast (~ps), the hysteresis process is slow and occurs on the ~100 s time scale. This slow building of the hysteresis probably indicates a change in the conformation disorder of the junctions and/or temperature of the junction. While we cannot definitively prove the tunnelling mechanism, confocal Raman measurements support a mechanism involving changes in molecular conformation or the effective temperature of the junction (Figure S11). Since incoherent tunneling involves thermally activated hopping and thermal relaxation of tunneling charge carriers, we suspect incoherent tunneling in the BIPY-$CoCl_2$ junctions leads to changes in the conformation structure of the SAMs and the observed hysteretic behavior.

CONCLUSIONS

This work describes the hysteresis of conductance in two-terminal molecular junctions based on alkanethiolates terminated by 2,2′-bipyridine complexed with first-row divalent transition metal ions. These BIPY-MCl_2 junctions are a model system for understanding hysteresis in molecular junctions: the hysteretic behavior in BIPY-MCl_2 junctions changes dramatically depending on the transition metal complexed to BIPY, while the core structure of the junctions remains the same. These characteristics of the BIPY-MCl_2 junctions allowed us to investigate effects that are purely electronic in nature.

Using this model system, we observed that BIPY-MCl_2 junctions (M = Mn(II), Fe(II), Co(II), and Ni(II)) measured within the voltage range of ±1.0 V have hysteretic behavior in the conductance, while the other junctions (M = Cr(II) and Cu(II)) do not. We also observed a correlation between the mechanism of tunneling and the occurrence of hysteresis. Specifically, BIPY-MCl_2 junctions entering the incoherent tunneling regime at a given applied voltage window *do* exhibit conductance hysteresis, while the BIPY-MCl_2 junctions that stay in the direct tunneling regime do not exhibit hysteresis. Using this correlation, we demonstrated that the hysteretic behavior in BIPY-MCl_2 junctions can be controlled by increasing or decreasing the voltage window, which restricts (or permits) the incoherent tunneling mechanism. This voltage-induced change of conductance demonstrates a simple, fast, and reversible way to modulate conductance in molecular tunneling junctions.

The magnitude of the hysteresis window in BIPY-MCl_2 junctions is positively correlated with the rectification ratio. This correlation supports our hypothesis and provides information on the shared properties of molecular rectifiers and molecular switches. This correlation will help to (i) understand and design rectifying memory devices, which require a dual functionality of bistable hysteretic behavior and rectification, and (ii) understand the electrical features (e.g., hysteresis) of molecular rectifiers comprising insulating and conducting moiety more deeply.

Relationships between hysteresis in conductance and the physical and electrical structure of molecular junctions are not well established in the field of molecular electronics. The presence of transition in conduction mechanism enables the prediction of the electrical characteristics of BIPY-MCl_2 whether the junctions switch or not because the MO energy levels relative to the Fermi level of the electrodes are directly related to the mechanism of tunneling. The casual relations between incoherent tunneling and hysteretic behavior at the molecular level are related to the challenging problems in the fields of molecular electronics: the effect of electrons transporting across the molecule on the electronic and/or physical structure of molecular junctions remains unclear and requires more in-depth theoretical studies and sophisticated experimental approaches.

EXPERIMENTAL SECTION

Preparation of BIPY-MCl_2 Junctions. The BIPY-containing SAMs, which consist of an insulating alkyl chain terminated by a BIPY moiety, were prepared using a previously reported procedure.[45] SAMs of $S(CH_2)_{11}$BIPY were formed by immersion of a smooth template-stripped (TS) gold surface (Au^{TS}) in 1.0 mM ethanolic solutions of thiol-terminated molecules for 18 h under a nitrogen atmosphere. The BIPY moieties were complexed with metal(II) chlorides by incubating the SAM within a 10 mM solution of metal(II) chloride in ethanol to form Au^{TS}-$S(CH_2)_{11}$BIPY-MCl_2 junctions, also under a nitrogen atmosphere for 18 h. After each immersion in EtOH, we gently rinsed the samples with ethanol for 1 min (~1 mL/min) to remove residue on the surface and dried the samples under a slow flow of nitrogen gas.

Characterization: *J*−*V* Measurements. We performed the measurements within 1 h of the samples being prepared. After placing the samples (Au^{TS}-$S(CH_2)_{11}$BIPY-M(II)Cl_2^-) on an antivibration table, we connected a grounded Au surface to the negative port of a source meter (6430 Sub-Femtoamp Remote SourceMeter, Keithley). A 10-μL Hamilton syringe containing eutectic indium−gallium (EGaIn, 75.5% Ga 24.5%, and superficial layer of GaO_x) alloy, serving as a top electrode, was controlled by a micromanipulator and was connected to the port of the source meter. We formed an EGaIn tip of conical shape by extruding an EGaIn drop from the syringe on a clean Si wafer[28,70] and bringing the EGaIn tip gently into contact with the samples (contact area ≈ 900 μm^2). A voltage was subsequently applied to the EGaIn tip (a positive voltage corresponds to EGaIn oxidizing, and negative voltage corresponds to EGaIn reducing), and the current flowing across the junctions was measured (one trace from 0 V to +1.0 V to −1.0 to 0 V).

ASSOCIATED CONTENT

Supporting Information

The Supporting Information is available free of charge at https://pubs.acs.org/doi/10.1021/acsnano.1c10155.

https://doi.org/10.1021/acsnano.1c10155
ACS Nano 2022, 16, 4206−4216

Details concerning nomenclature, details of experimental methods, energy diagrams describing coherent and incoherent tunneling conditions, determination of the structure of the BIPY-MCl_2 junctions using X-ray photoelectron spectroscopy, density functional theory, Raman spectroscopy, and general information (PDF)

AUTHOR INFORMATION

Corresponding Author

George M. Whitesides − *Department of Chemistry and Chemical Biology, Harvard University, Cambridge, Massachusetts 02138, United States;* orcid.org/0000-0001-9451-2442; Email: gwhitesides@gmwgroup.harvard.edu

Authors

Junwoo Park − *Department of Chemistry and Chemical Biology, Harvard University, Cambridge, Massachusetts 02138, United States; Department of Chemistry, Sogang University, Seoul 04107, Republic of Korea*

Mohamad S. Kodaimati − *Department of Chemistry and Chemical Biology, Harvard University, Cambridge, Massachusetts 02138, United States*

Lee Belding − *Department of Chemistry and Chemical Biology, Harvard University, Cambridge, Massachusetts 02138, United States*

Samuel E. Root − *Department of Chemistry and Chemical Biology, Harvard University, Cambridge, Massachusetts 02138, United States*

George C. Schatz − *Department of Chemistry, Northwestern University, Evanston, Illinois 60208-3113, United States;* orcid.org/0000-0001-5837-4740

Complete contact information is available at: https://pubs.acs.org/10.1021/acsnano.1c10155

Author Contributions

[⊥]J.P. and M.S.K. contributed equally to this work.

Notes

The authors declare no competing financial interest.

ACKNOWLEDGMENTS

This work was supported by the National Science Foundation (NSF, CHE-18083681 to G.M.W.) and by NSF through the Harvard University Materials Research Science and Engineering Center (MRSEC, DMR-1420570, and DMR-2011754). Sample characterization was performed in part at the Center for Nanoscale Systems (CNS) at Harvard University, a member of the National Nanotechnology Infrastructure Network (NNIN), which is supported by the National Science Foundation (ECS-0335765). DFT calculations were run on the FASRC Cannon cluster supported by the FAS Division of Science Research Computing at Harvard University. J.P. acknowledges the National Research Foundation of Korea (NRF) grant funded by the Korea government (2022R1C1C1006638), and the Sogang University Research Grant of 2021 (202110030.01). M.S.K. acknowledges the Simons Foundation, Award 290364FY21, for partial salary support. L.B. acknowledges fellowship support from NSERC, Canada. G.C.S. acknowledges the Department of Energy, Office of Basic Energy Sciences, Grant DE-SC0000989. We thank Victoria E. Campbell and Hyo Jae Yoon for their discussions.

REFERENCES

(1) Joachim, C.; Gimzewski, J. K.; Aviram, A. Electronics Using Hybrid-Molecular and Mono-Molecular Devices. *Nature* **2000**, *408*, 541.

(2) Carroll, R. L.; Gorman, C. B. The Genesis of Molecular Electronics. *Angew. Chemie Int. Ed.* **2002**, *41*, 4378−4400.

(3) McCreery, R. L. Molecular Electronic Junctions. *Chem. Mater.* **2004**, *16*, 4477−4496.

(4) Lortscher, E.; Gotsmann, B.; Lee, Y.; Yu, L.; Rettner, C.; Riel, H. Transport Properties of a Single-Molecule Diode. *ACS Nano* **2012**, *6*, 4931−4939.

(5) Ratner, M. A Brief History of Molecular Electronics. *Nat. Nanotechnol.* **2013**, *8*, 378−381.

(6) Bergfield, J. P.; Ratner, M. A. Forty Years of Molecular Electronics: Non-Equilibrium Heat and Charge Transport at the Nanoscale. *Phys. Status Solidi Basic Res.* **2013**, *250*, 2249−2266.

(7) Vilan, A.; Aswal, D.; Cahen, D. Large-Area, Ensemble Molecular Electronics: Motivation and Challenges. *Chem. Rev.* **2017**, *117*, 4248−4286.

(8) Casalini, S.; Bortolotti, C. A.; Leonardi, F.; Biscarini, F. Self-Assembled Monolayers in Organic Electronics. *Chem. Soc. Rev.* **2017**, *46*, 40−71.

(9) Quek, S. Y.; Kamenetska, M.; Steigerwald, M. L.; Choi, H. J.; Louie, S. G.; Hybertsen, M. S.; Neaton, J. B.; Venkataraman, L. Mechanically Controlled Binary Conductance Switching of a Single-Molecule Junction. *Nat. Nanotechnol.* **2009**, *4* (4), 230−234.

(10) Donhauser, Z. J.; Mantooth, B. A.; Kelly, K. F.; Bumm, L. A.; Monnell, J. D.; Stapleton, J. J.; Price, D. W.; Rawlett, A. M.; Allara, D. L.; Tour, J. M.; Weiss, P. S. Conductance Switching in Single Molecules through Conformational Changes. *Science* **2001**, *292*, 2303.

(11) Venkataraman, L.; Klare, J. E.; Nuckolls, C.; Hybertsen, M. S.; Steigerwald, M. L. Dependence of Single-Molecule Junction Conductance on Molecular Conformation. *Nature* **2006**, *442*, 904−907.

(12) Goswami, S.; Rath, S. P.; Thompson, D.; Hedström, S.; Annamalai, M.; Pramanick, R.; Ilic, B. R.; Sarkar, S.; Hooda, S.; Nijhuis, C. A.; Martin, J.; Williams, R. S.; Goswami, S.; Venkatesan, T. Charge Disproportionate Molecular Redox for Discrete Memristive and Memcapacitive Switching. *Nat. Nanotechnol.* **2020**, *15*, 380−389.

(13) Schwarz, F.; Koch, M.; Kastlunger, G.; Berke, H.; Stadler, R.; Venkatesan, K.; Lörtscher, E. Charge Transport and Conductance Switching of Redox-Active Azulene Derivatives. *Angew. Chemie - Int. Ed.* **2016**, *55*, 11781−11786.

(14) McCreery, R.; Dieringer, J.; Solak, A. O.; Snyder, B.; Nowak, A. M.; McGovern, W. R.; DuVall, S. Molecular Rectification and Conductance Switching in Carbon-Based Molecular Junctions by Structural Rearrangement Accompanying Electron Injection. *J. Am. Chem. Soc.* **2003**, *125*, 10748−10758.

(15) Chen, J.; Su, J.; Wang, W.; Reed, M. A. Electronic Memory Effects in Self-Assembled Monolayer Systems. *Phys. E Low-Dimensional Syst. Nanostructures* **2003**, *16*, 17−23.

(16) Brooke, R. J.; Szumski, D. S.; Vezzoli, A.; Higgins, S. J.; Nichols, R. J.; Schwarzacher, W. Dual Control of Molecular Conductance through Ph and Potential in Single-Molecule Devices. *Nano Lett.* **2018**, *18*, 1317−1322.

(17) Wagner, S.; Kisslinger, F.; Ballmann, S.; Schramm, F.; Chandrasekar, R.; Bodenstein, T.; Fuhr, O.; Secker, D.; Fink, K.; Ruben, M.; Weber, H. B. Switching of a Coupled Spin Pair in a Single-Molecule Junction. *Nat. Nanotechnol.* **2013**, *8*, 575−579.

(18) Kronemeijer, A. J.; Akkerman, H. B.; Kudernac, T.; Van Wees, B. J.; Feringa, B. L.; Blom, P. W. M.; De Boer, B. Reversible Conductance Switching in Molecular Devices. *Adv. Mater.* **2008**, *20*, 1467−1473.

(19) Van Der Molen, S. J.; Liao, J.; Kudernac, T.; Agustsson, J. S.; Bernard, L.; Calame, M.; Van Wees, B. J.; Feringa, B. L.; Schönenberger, C. Light-Controlled Conductance Switching of Ordered Metal-Molecule-Metal Devices. *Nano Lett.* **2009**, *9*, 76−80.

(20) Liljeroth, P.; Repp, J.; Meyer, G. Current-Induced Hydrogen Tautomerization and Conductance Switching of Naphthalocyanine Molecules. *Science (80-.)* **2007**, *317*, 1203−1206.

(21) Blum, A. S.; Kushmerick, J. G.; Long, D. P.; Patterson, C. H.; Yang, J. C.; Henderson, J. C.; Yao, Y.; Tour, J. M.; Shashidhar, R.; Ratna, B. R. Molecularly Inherent Voltage-Controlled Conductance Switching. *Nat. Mater.* **2005**, *4*, 167−172.
(22) Han, Y.; Nickle, C.; Zhang, Z.; Astier, H. P. A. G.; Duffin, T. J.; Qi, D.; Wang, Z.; del Barco, E.; Thompson, D.; Nijhuis, C. A. Electric-Field-Driven Dual-Functional Molecular Switches in Tunnel Junctions. *Nat. Mater.* **2020**, *19*, 843−848.
(23) Gaudioso, J.; Lauhon, L. J.; Ho, W. Vibrationally Mediated Negative Differential Resistance in a Single Molecule. *Phys. Rev. Lett.* **2000**, *85*, 1918−1921.
(24) Pathem, B. K.; Claridge, S. A.; Zheng, Y. B.; Weiss, P. S. Molecular Switches and Motors on Surfaces. *Annu. Rev. Phys. Chem.* **2013**, *64*, 605−630.
(25) Zhang, J. L.; Zhong, J. Q.; Lin, J. D.; Hu, W. P.; Wu, K.; Xu, G. Q.; Wee, A. T. S.; Chen, W. Towards Single Molecule Switches. *Chem. Soc. Rev.* **2015**, *44* (10), 2998−3022.
(26) Belding, L.; Root, S. E.; Li, Y.; Park, J.; Baghbanzadeh, M.; Rojas, E.; Pieters, P. F.; Yoon, H. J.; Whitesides, G. M. Conformation, and Charge Tunneling through Molecules in SAMs. *J. Am. Chem. Soc.* **2021**, *143*, 3481−3493.
(27) Weiss, E. A.; Kaufman, G. K.; Kriebel, J. K.; Li, Z.; Schalek, R.; Whitesides, G. M. Si/SiO2-Templated Formation of Ultraflat Metal Surfaces on Glass, Polymer, and Solder Supports: Their Use as Substrates for Self-Assembled Monolayers. *Langmuir* **2007**, *23*, 9686−9694.
(28) Chiechi, R. C.; Weiss, E. A.; Dickey, M. D.; Whitesides, G. M. Eutectic Gallium-Indium (EGaIn): A Moldable Liquid Metal for Electrical Characterization of Self-Assembled Monolayers. *Angew. Chemie - Int. Ed.* **2008**, *47*, 142−144.
(29) Rothemund, P.; Morris Bowers, C.; Suo, Z.; Whitesides, G. M. Influence of the Contact Area on the Current Density across Molecular Tunneling Junctions Measured with EGaIn Top-Electrodes. *Chem. Mater.* **2018**, *30*, 129−137.
(30) Sodhi, R. N. S.; Brodersen, P.; Cademartiri, L.; Thuo, M. M.; Nijhuis, C. A. Surface and Buried Interface Layer Studies on Challenging Structures as Studied by ARXPS. *Surf. Interface Anal.* **2017**, *49*, 1309−1315.
(31) Häkkinen, H. The Gold-Sulfur Interface at the Nanoscale. *Nat. Chem.* **2012**, *4*, 443−455.
(32) Park, J.; Belding, L.; Yuan, L.; Mousavi, M. P. S.; Root, S. E.; Yoon, H. J.; Whitesides, G. M. Rectification in Molecular Tunneling Junctions Based on Alkanethiolates with Bipyridine-Metal Complexes. *J. Am. Chem. Soc.* **2021**, *143*, 2156−2163.
(33) Burr, G. W.; Shenoy, R. S.; Virwani, K.; Narayanan, P.; Padilla, A.; Kurdi, B.; Hwang, H. Access Devices for 3D Crosspoint Memory. *J. Vac. Sci. Technol. B, Nanotechnol. Microelectron. Mater. Process. Meas. Phenom.* **2014**, *32*, 040802.
(34) Seminario, J. M.; Zacarias, A. G.; Tour, J. M. Theoretical Study of a Molecular Resonant Tunneling Diode. *J. Am. Chem. Soc.* **2000**, *122*, 3015−3020.
(35) Di Ventra, M.; Kim, S. G.; Pantelides, S. T.; Lang, N. D. Temperature Effects on the Transport Properties of Molecules. *Phys. Rev. Lett.* **2001**, *86*, 288.
(36) Cornil, J.; Karzazi, Y.; Brédas, J. L. Negative Differential Resistance in Phenylene Ethynylene Oligomers. *J. Am. Chem. Soc.* **2002**, *124*, 3516−3517.
(37) Lang, N. D.; Avouris, P. Electrical Conductance of Parallel Atomic Wires. *Phys. Rev. B Condens. Matter Mater. Phys.* **2000**, *62*, 7325.
(38) Ramachandran, G. K.; Hopson, T. J.; Rawlett, A. M.; Nagahara, L. A.; Primak, A.; Lindsay, S. M. A Bond-Fluctuation Mechanism for Stochastic Switching in Wired Molecules. *Science* **2003**, *300*, 1413−1416.
(39) Moore, A. M.; Dameron, A. A.; Mantooth, B. A.; Smith, R. K.; Fuchs, D. J.; Ciszek, J. W.; Maya, F.; Yao, Y.; Tour, J. M.; Weiss, P. S. Molecular Engineering and Measurements to Test Hypothesized Mechanisms in Single Molecule Conductance Switching. *J. Am. Chem. Soc.* **2006**, *128*, 1959−1967.
(40) Kaes, C.; Katz, A.; Hosseini, M. W. Bipyridine: The Most Widely Used Ligand. A Review of Molecules Comprising at Least Two 2,2′-Bipyridine Units. *Chem. Rev.* **2000**, *100*, 3553−3590.
(41) Park, J.; Belding, L.; Yuan, L.; Mousavi, M. P. S.; Root, S. E.; Yoon, H. J.; Whitesides, G. M. Rectification in Molecular Tunneling Junctions Based on Alkanethiolates with Bipyridine-Metal Complexes. *J. Am. Chem. Soc.* **2021**, *143* (143), 2156−2163.
(42) Trouwborst, M. L.; Martin, C. A.; Smit, R. H. M.; Guédon, C. M.; Baart, T. A.; van der Molen, S. J.; van Ruitenbeek, J. M. Transition Voltage Spectroscopy and the Nature of Vacuum Tunneling. *Nano Lett.* **2011**, *11*, 614.
(43) Joachim, C.; Ratner, M. A. Molecular Electronics: Some Views on Transport Junctions and Beyond. *Proc. Natl. Acad. Sci. U. S. A.* **2005**, *102*, 8801−8808.
(44) Metzger, R. M. Electrical Rectification by a Molecule: The Advent of Unimolecular Electronic Devices. *Acc. Chem. Res.* **1999**, *32*, 950−957.
(45) Ashwell, G. J.; Urasinska, B.; Tyrrell, W. D. Molecules That Mimic Schottky Diodes. *Phys. Chem. Chem. Phys.* **2006**, *8*, 3314−3319.
(46) Nijhuis, C. A.; Reus, W. F.; Whitesides, G. M. Molecular Rectification in Metal-SAM-Metal Oxide-Metal Junctions. *J. Am. Chem. Soc.* **2009**, *131*, 17814−17827.
(47) Yoon, H. J.; Liao, K. C.; Lockett, M. R.; Kwok, S. W.; Baghbanzadeh, M.; Whitesides, G. M. Rectification in Tunneling Junctions: 2,2′-Bipyridyl-Terminated n -Alkanethiolates. *J. Am. Chem. Soc.* **2014**, *136*, 17155−17162.
(48) Lopez-Villanueva, J. A.; Jimenez-Tejada, J. A.; Cartujo, P.; Bausells, J.; Carceller, J. E. Analysis of the Effects of Constant-Current Fowler-Nordheim-Tunneling Injection with Charge Trapping inside the Potential Barrier. *J. Appl. Phys.* **1991**, *70*, 3712−3720.
(49) DiMaria, D. J.; Cartier, E.; Arnold, D. Impact Ionization, Trap Creation, Degradation, and Breakdown in Silicon Dioxide Films on Silicon. *J. Appl. Phys.* **1993**, *73*, 3367−3384.
(50) Ku, P. S.; Schroder, D. K. Charges Trapped Throughout the Oxide and Their Impact on the Fowler-Nordheim Current in MOS Devices. *IEEE Trans. Electron Devices* **1994**, *41*, 1669−1672.
(51) Jiang, J.; Awadelkarim, O. O.; Chan, Y. D. A Study of Carrier-Trap Generation by Fowler-Nordheim Tunneling Stress on Poly-crystalline-Silicon/SiO2/Silicon Structures. *Solid-State Electron.* **1997**, *41*, 41−46.
(52) Chen, T. P.; Li, S.; Fung, S.; Lo, K. F. Interface Trap Generation by FN Injection under Dynamic Oxide Field Stress. *IEEE Trans. Electron Devices* **1998**, *45*, 1920−1926.
(53) Yan, C.; Yuan, R.; Pfalzgraff, W. C.; Nishida, J.; Wang, L.; Markland, T. E.; Fayer, M. D. Unraveling the Dynamics and Structure of Functionalized Self-Assembled Monolayers on Gold Using 2D IR Spectroscopy and MD Simulations. *Proc. Natl. Acad. Sci. U. S. A.* **2016**, *113*, 4929−4934.
(54) Stranick, S. J.; Parikh, A. N.; Tao, Y.-T.; Allara, D. L.; Weiss, P. S. Phase Separation of Mixed-Composition Self-Assembled Monolayers into Nanometer Scale Molecular Domains. *J. Phys. Chem.* **1994**, *98*, 7636−7646.
(55) Badia, A.; Lennox, R. B.; Reven, L. A Dynamic View of Self-Assembled Monolayers. *Acc. Chem. Res.* **2000**, *33*, 475−481.
(56) Ward, D. R.; Corley, D. A.; Tour, J. M.; Natelson, D. Vibrational and Electronic Heating in Nanoscale Junctions. *Nat. Nanotechnol.* **2011**, *6*, 33.
(57) Tsutsui, M.; Taniguchi, M.; Kawai, T. Local Heating in Metal−Molecule−Metal Junctions. *Nano Lett.* **2008**, *8*, 3293−3297.
(58) D'Agosta, R.; Sai, N.; Di Ventra, M. Local Electron Heating in Nanoscale Conductors. *Nano Lett.* **2006**, *6*, 2935−2938.
(59) Huang, Z.; Xu, B.; Chen, Y.; Di Ventra, M.; Tao, N. Measurement of Current-Induced Local Heating in a Single Molecule Junction. *Nano Lett.* **2006**, *6*, 1240.
(60) Huang, Z.; Chen, F.; D'agosta, R.; Bennett, P. A.; Di Ventra, M.; Tao, N. Local Ionic and Electron Heating in Single-Molecule Junctions. *Nat. Nanotechnol.* **2007**, *2*, 698−703.

https://doi.org/10.1021/acsnano.1c10155
ACS Nano 2022, 16, 4206−4216

(61) Wang, R. Y.; Segalman, R. A.; Majumdar, A. Room Temperature Thermal Conductance of Alkanedithiol Self-Assembled Monolayers. *Appl. Phys. Lett.* **2006**, *89*, 173113.
(62) Mosso, N.; Drechsler, U.; Menges, F.; Nirmalraj, P.; Karg, S.; Riel, H.; Gotsmann, B. Heat Transport through Atomic Contacts. *Nat. Nanotechnol.* **2017**, *12*, 430−433.
(63) Cui, L.; Hur, S.; Akbar, Z. A.; Klöckner, J. C.; Jeong, W.; Pauly, F.; Jang, S.-Y.; Reddy, P.; Meyhofer, E. Thermal Conductance of Single-Molecule Junctions. *Nature* **2019**, *572*, 628−633.
(64) Klöckner, J. C.; Bürkle, M.; Cuevas, J. C.; Pauly, F. Length Dependence of the Thermal Conductance of Alkane-Based Single-Molecule Junctions: An Ab Initio Study. *Phys. Rev. B* **2016**, *94*, 205425.
(65) Yan, X.; Li, P.; Yang, L.; Liu, J. Time-Dependent SERS Spectra Monitoring the Dynamic Adsorption Behavior of Bipyridine Isomerides Combined with Bianalyte Method. *Analyst* **2016**, *141*, 5189−5194.
(66) Moissette, A.; Batonneau, Y.; Brémard, C. Conformation and Protonation of 2,2′-Bipyridine and 4,4′-Bipyridine in Acidic Aqueous Media and Acidic ZSM-5 Zeolites: A Raman Scattering Study. *J. Am. Chem. Soc.* **2001**, *123*, 12325−12334.
(67) Keller, E. L.; Frontiera, R. R. Ultrafast Nanoscale Raman Thermometry Proves Heating Is Not a Primary Mechanism for Plasmon-Driven Photocatalysis. *ACS Nano* **2018**, *12*, 5848−5855.
(68) Sun, Y.; Yanagisawa, M.; Kunimoto, M.; Nakamura, M.; Homma, T. Estimated Phase Transition and Melting Temperature of APTES Self-Assembled Monolayer Using Surface-Enhanced Anti-Stokes and Stokes Raman Scattering. *Appl. Surf. Sci.* **2016**, *363*, 572−577.
(69) Du, C.; Norris, S. R.; Thakur, A.; Chen, J.; Vanveller, B.; Thuo, M. Molecular Conformation in Charge Tunneling across Large-Area Junctions. *J. Am. Chem. Soc.* **2021**, *143*, 13878−13886.
(70) Simeone, F. C.; Yoon, H. J.; Thuo, M. M.; Barber, J. R.; Smith, B. S.; Whitesides, G. M. Defining the Value of Injection Current and Effective Electrical Contact Area for EGaIn-Based Molecular Tunneling Junctions. *J. Am. Chem. Soc.* **2013**, *135*, 18131−18144.

https://doi.org/10.1021/acsnano.1c10155
ACS Nano 2022, 16, 4206−4216